Ruthenium monoterpyridine complexes incorporating α,α′-diimine based ancillary functions. Synthesis, crystal structure, spectroelectrochemical properties and catalytic aspect

Nripen Chanda [a], Biplab Mondal [a], Vedavati G. Puranik [b], Goutam Kumar Lahiri [a,*]

[a] *Department of Chemistry, Indian Institute of Technology-Bombay, Powai, Mumbai 400 076, India*
[b] *Physical Chemistry Division, National Chemistry Laboratory, Pune, Maharashtra 411 008, India*

Abstract

Ruthenium monoterpyridine complexes of the type $[Ru^{II}(trpy)(L')(X)](ClO_4)_m \cdot 2H_2O$ (**1**–**2**) [trpy = 2,2′:6′,2″-terpyridine; L′ = $NC_5H_4C(H)=N(C_6H_4)_nNH_2$ ($n = 1$ and 2); X = Cl^-, $m = 1$ (**1**); X = H_2O, $m = 2$ (**2**)] have been synthesized via the selective hydrolysis of one of the imine functions present in the preformed stable dinucleating bridging functions, $NC_5H_4C(H)=N(C_6H_4)_nN=C(H)H_4C_5N$ (L) ($n = 1$, 2). The single crystal X-ray structures of the dinucleating bridging function (L^1) and the chloro complex (**1a**) (in both cases $n = 1$) have been determined. The complexes stabilize preferentially in one particular isomeric form where the Cl^- or H_2O molecule is in the *trans* configuration with respect to the N(imine) center. The chloro complexes (**1**) exhibit strong MLCT bands near 500 nm whereas in the case of the aqua complexes (**2**) the MLCT bands are blue shifted near 470 nm. The chloro complexes (**1**) exhibit weak emissions in EtOH–MeOH (4:1 v/v) glass at 77 K near 600 nm (quantum yield, $\Phi_{em} = 0.015$–0.03). In acetonitrile solvent **1** display a ruthenium(III)–ruthenium(II) couple near 0.8 V and terpyridine based reduction near 1 V versus SCE. The aqua complexes (**2**) exhibit a concerted $2e^-/2H^+$ oxidation process in the acidic region and in the alkaline region, the complexes display a $2e^-/H^+$ oxidation process. The potentials are observed to decrease linearly with the increase in pH. The proton coupled redox processes in the acidic and basic regions correspond to $[Ru^{II}(trpy)(L')(H_2O)]^{2+}$–$[Ru^{IV}(trpy)(L')(O)]^{2+}$ and $[Ru^{II}(trpy)(L')(OH)]^{+}$–$[Ru^{IV}(trpy)(L')(O)]^{2+}$ couples, respectively. The chemical oxidation of **2** by excess Ce^{IV} solution in 1 (N) H_2SO_4 also leads to the formation of the corresponding $[Ru^{IV}(trpy)(L')(O)]^{2+}$ (**3**). The oxo complexes (**3**) are stable only in the presence of excess Ce^{IV} ion, otherwise they slowly catalyze the oxidation of water to dioxygen and return back to the parent aqua species. The electrochemically generated oxo-species are found to catalyze the benzyl alcohol oxidation process.

Keywords: Ruthenium monoterpyridine complexes; Ancillary functions; Crystal structures

1. Introduction

Ruthenium polypyridine (bipyridine and terpyridine) complexes have received considerable research interest in recent years primarily due to their strong metal to ligand charge-transfer transitions, facile electron-transfer properties and long lived ^{3}MLCT excited states and these in combination make them attractive for designing photo- and electrochemical devices [1–13]. In recent years, it has been observed that the electronic nature of the ancillary functions in the ruthenium monoterpyridine core plays an important role in directing the chemical and electrochemical properties of this class of complexes [14–21] and this has initiated the present program of developing a newer class of ruthenium monoterpyridine derivatives incorporating the α,α′-diimine based ancillary functions. Since the present trend in this direction has been primarily focussed towards the framing of multinuclear to supramolecular assemblies [22–27], we had taken the program of synthesizing

dinuclear ruthenium terpyridine complexes using the α,α′-diimine based neutral bridging functions NC_5H_4–CH=N–$(C_6H_4)_n$–N=CH–H_4C_5N ($n = 1$, 2), L. Although the bridging functions (L) are stable enough in the free state [28,29], during the reaction with $Ru(trpy)Cl_3$ (trpy = 2,2′:6,2″-terpyridine) one of the imine functions of L has been selectively hydrolyzed. This in turn leads to the formation of ruthenium monoterpyridine complexes of the type $[Ru^{II}(trpy)(L')Cl]^+$ (**1**) where L′ corresponds to NC_5H_4–CH=N–$(C_6H_4)_n$–NH_2 ($n = 1$, 2).

Herein we report the stepwise syntheses of the complexes, $[Ru^{II}(trpy)(L')Cl]^+$ (**1**) → $[Ru^{II}(trpy)(L')H_2O]^{2+}$ (**2**) → $[Ru^{IV}(trpy)(L')O]^{2+}$ (**3**), crystal structures of L^1 and **1a**, and the chemical–electrochemical reactivities of the complexes including the catalytic/electrocatalytic behaviors of the in situ generated oxo species (**3**). The specific role of the electronic nature of L′ in **1**–**3** in comparison with the analogous ancillary functions present in other known ruthenium monoterpyridine complexes have been noted.

2. Experimental

2.1. Materials

The starting complex $Ru(trpy)Cl_3$ and the ligands L^{1-2} were prepared according to the reported procedures [30,28]. 2,2′:6,2″-terpyridine was obtained from Aldrich, USA. Other chemicals and solvents were reagent grade and used as received. Alumina (neutral) was used for column chromatography. For spectroscopic and electrochemical studies HPLC grade solvents were used. Water of high purity was obtained by distillation of the deionized water from $KMnO_4$. Sodium perchlorate for electrochemical work in aqueous medium was recrystallized from water.

2.2. Physical measurements

UV–Vis spectra were recorded by using a Shimadzu-2100 spectrophotometer. FT-IR spectra were taken on a Nicolet spectrophotometer with samples prepared as KBr pellets. Solution electrical conductivity was checked using a Systronic 305 conductivity bridge. Magnetic susceptibility was checked with a PAR vibrating sample magnetometer. NMR spectra were obtained with a 300 MHz Varian FT spectrometer. Cyclic voltammetric, differential pulse voltammetric and coulometric measurements were carried out using a PAR model 273A electrochemistry system. Platinum wire working and auxiliary electrodes and an aqueous saturated calomel reference electrode (SCE) were used in a three-electrode configuration. The supporting electrolyte was $[NEt_4]ClO_4$ and the solute concentration was approximately 10^{-3} M. The half-wave potential E°_{298} was set equal to $0.5(E_{pa} + E_{pc})$, where E_{pa} and E_{pc} are anodic and cathodic cyclic voltammetric peak potentials, respectively. A Pt wire-gauze working electrode was used in coulometric experiments. All experiments were carried out under a dinitrogen atmosphere and were uncorrected for junction potentials. The elemental analyses were carried out with a Carlo–Erba (Italy) elemental analyzer. Solution emission properties were checked using a SPEX-fluorolog spectrofluorometer. X-ray data were collected by using a Nonius MACH 3 four-circle diffractometer with graphite monochromated Mo Kα radiation ($\lambda = 0.71073$ Å).

2.3. Preparation of complexes

The complexes $[Ru(trpy)(L')(Cl)](ClO_4)\cdot 2H_2O$ (**1a** and **1b**) were prepared by following a general procedure. Details are mentioned for the complex **1a**.

2.4. $[Ru(trpy)(L')(Cl)]ClO_4\cdot 2H_2O$ (1a)

The starting complex $Ru(trpy)Cl_3$ (100 mg, 0.227 mmol) was taken in 25 ml of hot EtOH. The preformed bridging ligand L^1 (65 mg, 0.228 mmol) was added to the above solution and the mixture was heated to reflux for 14 h. The solvent was removed under reduced pressure. The residual mass was dissolved in a minimum volume of MeCN and saturated aq. $NaClO_4$ solution was added. The solid product thus obtained on cooling was filtered and washed with ice-cold water followed by cold EtOH. The crude product was purified by using an alumina (neutral) column. Initially the side product, $[Ru(trpy)_2](ClO_4)_2\cdot 2H_2O$ was eluted by CH_2Cl_2–MeCN (5:2) mixture. The pink colored complex, **1a** was eluted by CH_2Cl_2–MeCN (5:3) mixture. Another fraction of the pink solution corresponding to **1a** was eluted later by CH_2Cl_2–MeCN (1:1) from the same column. The complex **1a** thus obtained from the two different batches were further purified separately by following the same above procedures in order to remove any trace of $[Ru(trpy)_2](ClO_4)_2\cdot 2H_2O$ impurity. Similarly the $[Ru(trpy)_2](ClO_4)_2\cdot 2H_2O$ complex obtained from the above column was also purified again in order to make it free from **1a**. The two pink colored solutions thus obtained separately from the same column were found to exhibit identical spectral and electrochemical features. Evaporation of the solvent mixture resulted in pure solid complexes, **1a** and $[Ru(trpy)_2](ClO_4)_2\cdot 2H_2O$. Yield: **1a** (95.0 mg, 61%) and $[Ru(trpy)_2](ClO_4)_2\cdot 2H_2O$ (15 mg, 10%). *Anal*. Calc. for **1a**: C, 46.15; H, 3.73; N, 11.97. Found: C, 46.31; H, 3.45; N, 12.22%. Λ_M/Ω^{-1} ($cm^2\ mol^{-1}$) in MeCN at 298 K: 148. *Anal*. Calc. for **1b**: C, 50.90; H, 3.89; N, 10.80. Found: C, 50.52; H, 3.32; N, 11.02%. Λ_M/Ω^{-1} ($cm^2\ mol^{-1}$) in MeCN at 298 K: 140.

2.5. [Ru(trpy)(L′)(H$_2$O)](ClO$_4$)$_2$·2H$_2$O (2a)

The aqua complexes (**2**) were prepared from the corresponding chloro species using excess $AgNO_3$. Details are mentioned for **2a**.

Silver nitrate (120 mg, 0.70 mmol) was added to the aqueous solution of the chloro complex, [Ru(trpy)(L′)(Cl)]ClO$_4$·2H$_2$O (**1a**) (100 mg, 0.14 mmol in 15 ml water) and the solution was heated to reflux for 2.5 h. It was then cooled and the precipitated AgCl was filtered off through a sintered glass crucible (G-4). The volume of the filtrate was reduced to 5 ml and saturated aq. $NaClO_4$ solution was added to it. The mixture was kept in the refrigerator overnight. The solid product (**2a**) thus obtained was filtered and washed with ice-cold water and dried in vacuo over P_4O_{10}. Yield: 78 mg (70%). *Anal*. Calc. for **2a**: C, 41.34; H, 3.60; N, 10.71. Found: C, 40.92; H, 3.33; N, 10.37%. Λ_M/Ω^{-1} (cm^2 mol^{-1}) in MeCN at 298 K: 230. *Anal*. Calc. for **2b**: C, 46.06; H, 3.75; N, 9.77. Found: C, 46.59; H, 3.43; N, 10.11%. Λ_M/Ω^{-1} (cm^2 mol^{-1}) in MeCN at 298 K: 240.

2.6. X-ray structure determination

The single crystals of L^1 were grown by slow diffusion of a CH_2Cl_2 solution of L^1 in C_6H_{14} followed by slow evaporation. The single crystals of **1a** were obtained by slow diffusion of the MeCN solution of **1a** in C_6H_6 followed by slow evaporation. Significant crystal data and data collection parameters are listed in Table 1. The structures were solved by direct methods using SHELXS-86 and refined by full-matrix least-squares on F^2 using SHELXL-97 [31].

Table 1
Crystallographic data for NC$_5$H$_4$–CH=N–(C$_6$H$_4$)–N=CH–H$_4$C$_5$N (L^1) and [Ru^{II}(trpy){NC$_5$H$_4$–CH=N–C$_6$H$_4$–NH$_2$}Cl]ClO$_4$ (**1a**)

	L^1	**1a**
Empirical formula	$C_9H_7N_2$	$C_{27}H_{22}N_6Cl_2O_4Ru$
M	143.17	666.48
Crystal symmetry	monoclinic	monoclinic
Space group	$P2_1/a$	$P2_1/n$
a (Å)	11.5290 (14)	8.4410 (10)
b (Å)	4.8118 (6)	13.884 (2)
c (Å)	13.7074 (14)	23.673 (4)
β (°)	109.14 (1)	98.710 (10)
V (Å^3)	718.39 (14)	2742.4 (7)
Z	4	4
μ (mm^{-1})	0.082	0.812
R_1	0.0403	0.0877
wR_2	0.0940	0.0999

3. Results and discussion

3.1. Synthesis

The bridging ligands L^1–L^2, used for the present study differ primarily with respect to the length of the spacers (Scheme 1). The ligands are designed with the intention of holding two Ru(trpy)Cl units through the terminal N_p (N_p = pyridine nitrogen) and N_i (N_i = imine nitrogen) donor centers of L. However, the reaction of L with the starting complex Ru(trpy)Cl$_3$ in a 1:2 mole ratio in ethanol solvent results in a monomeric species of the type [Ru(trpy)(L′)Cl]$^+$, **1** where L′ corresponds to $NC_5H_4CH{=}N{-}(C_6H_4)_n{-}NH_2$ ($n = 1$, **1a**; $n = 2$, **1b**) (Scheme 1).

During the course of the reaction one of the imine functions of the preformed bridging ligands (L) has been selectively hydrolyzed and the resulting mononucleating fragment of the bridging moiety (L′) leads to the formation of **1** (Scheme 1). The complexes have been isolated as their dihydrated perchlorate salts, [Ru^{II}(trpy)(L′)Cl]ClO$_4$·2H$_2$O (**1**).

Under identical reaction conditions (Scheme 1) but in the absence of ruthenium precursor Ru(trpy)Cl$_3$, the preformed bridging functions (L) are found to remain intact, implying the effective role of the metal fragment in transforming L → L′ in **1**.

The synthesis of **1** by using a 1:2 mole ratio of L and Ru(trpy)Cl$_3$ is always observed to be accompanied by the formation of a [Ru(trpy)$_2$]$^{2+}$ complex in an approximately 1:1 ratio. However, the use of a 1:1 mole ratio of L and Ru(trpy)Cl$_3$ reduces the yield of [Ru(trpy)$_2$]$^{2+}$ to an appreciable extent {**1**–[Ru(trpy)$_2$]$^{2+}$, 6:1, Section 2}. In order to minimize the perpetual formation of the undesired product [Ru(trpy)$_2$]$^{2+}$, the 1:1 mole ratio of L and Ru(trpy)Cl$_3$ had always been selectively used.

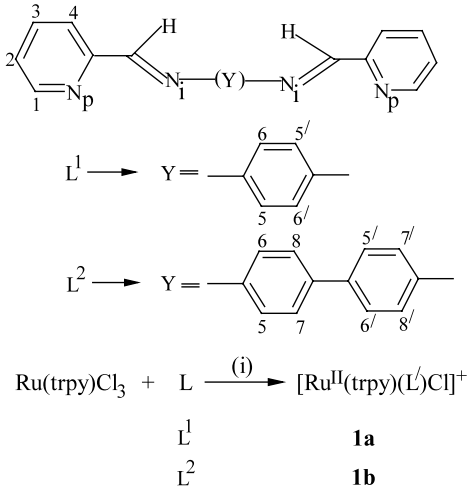

Scheme 1. (i) EtOH, heating, N_2.

Although the unsymmetrical nature of L′ in **1** leads to the possibility of the simultaneous formation of two isomers **A** and **B**, here the reaction (Scheme 1) systematically results in one particular isomeric product (see NMR). The existence of the isomeric form **B** has been confirmed by single-crystal X-ray structure for **1a** (see later). Based on the similar spectral features of **1a** and **1b** (see later), we believe that the complex **1b** also exists in same isomeric form **B**.

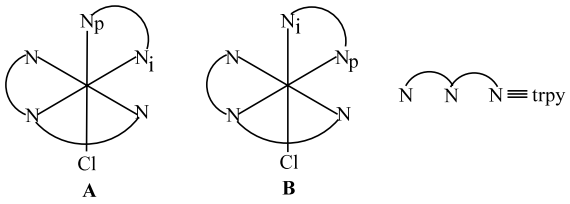

The aqua complexes $[Ru^{II}(trpy)(L')(H_2O)]^{2+}$ (**2**) have been isolated as their dihydrated perchlorate salts from the corresponding chloro complexes (**1**) in the presence of excess aqueous $AgNO_3$.

The oxo-complexes $[Ru^{IV}(trpy)(L')(O)]^{2+}$ (**3**) can be generated in solution state by chemical oxidation of the aqua species (**2**) using excess ceric solution in 1 (N) H_2SO_4. The isolation of the pure oxo derivative (**3**) in the solid state has not been successful as in the absence of Ce^{IV} ion the oxo-species reduces back to the parent aqua species (see later).

The isolated chloro (**1**) and aqua (**2**) complexes are diamagnetic and show 1:1 and 1:2 conductivities, respectively (Section 2). The complexes exhibit satisfactory elemental analyses (Section 2).

3.2. *Crystal structures of $NC_5H_4CH{=}N{-}(C_6H_4){-}N{=}CHC_5H_4N$ (L^1) and $[Ru(trpy)(L')Cl](ClO_4)$ (**1a**)*

The single crystal X-ray structure of L^1 is shown in Fig. 1. It shows that each half of the molecule is related to the other half by symmetry. Selective bond distances and angles are listed in Table 2. The bond distances and angles match well with the standard values.

The crystal structure of $[Ru(trpy)(L')Cl](ClO_4)$ (**1a**) is shown in Fig. 2. Selective bond distances and angles are listed in Table 2. The terpyridine group coordinates to the ruthenium center in a meridional fashion with the ligand L′ in a *cis* orientation. The chloride ligand is *trans* to the imine nitrogen (N_i) of L′ (structure **B**). The central Ru–N(1) distance [1.978(9) Å] of terpyridine is shorter than the terminal Ru–N(2)/Ru–N(3) distances, 2.080(9) Å [14–16]. Correspondingly, the geometrical strain of the meridionally disposed terpyridine ligand is reflected in the short *trans* angle, 159.0(4)° [14–16]. The Ru^{II}–N(5) [imine nitrogen, 2.057(10) Å], Ru–N(4) [pyridine nitrogen of L′, 2.097(10) Å] and Ru^{II}–Cl [2.414(3) Å] distances in **1a** are in agreement with those of reported similar complexes [16–20,32,33].

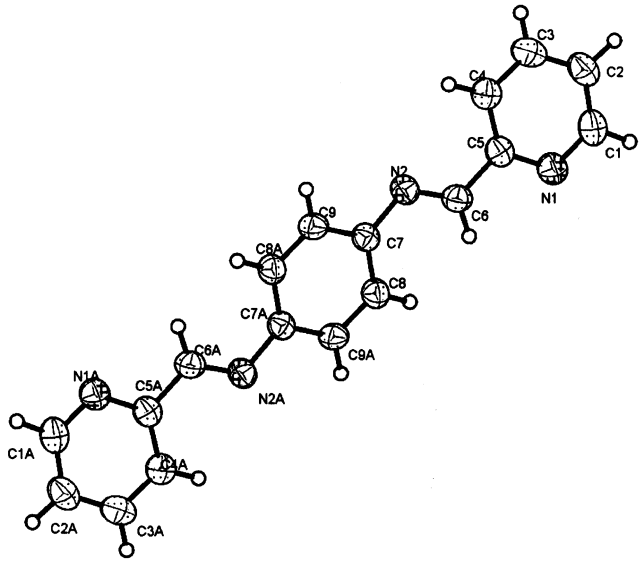

Fig. 1. An ORTEP diagram for $NC_5H_4CH{=}N{-}C_6H_4{-}N{=}CHC_5H_4N$, L^1. Atoms are drawn at 50% probability.

Table 2
Selected bond distances (Å) and angles (°) and their standard deviations for L^1 and **1a**

L^1		**1a**	
Bond distances			
N(1)–C(1)	1.335(2)	Ru–N(1)	1.978(9)
N(1)–C(5)	1.343(2)	Ru–N(2)	2.080(9)
N(2)–C(6)	1.264(2)	Ru–N(3)	2.080(9)
N(2)–C(7)	1.424(2)	Ru–N(4)	2.097(10)
C(4)–C(5)	1.384(2)	Ru–N(5)	2.057(10)
C(5)–C(6)	1.473(2)	Ru–Cl(1)	2.414(3)
		N(5)–C(21)	1.306(12)
Bond angles			
C(6)–N(2)–C(7)	119.90(16)	N(1)–Ru–N(5)	99.5(4)
N(1)–C(5)–C(6)	114.79(16)	N(1)–Ru–N(3)	79.7(5)
C(4)–C(5)–C(6)	122.45(17)	N(5)–Ru–N(3)	89.7(3)
N(2)–C(6)–C(5)	123.16(17)	N(1)–Ru–N(2)	79.4(4)
		N(5)–Ru–N(2)	95.6(3)
		N(3)–Ru–N(2)	159.0(4)
		N(1)–Ru–N(4)	176.1(4)
		N(5)–Ru–N(4)	77.6(4)
		N(2)–Ru–N(4)	103.4(4)
		N(1)–Ru–Cl(1)	89.5(3)
		N(5)–Ru–Cl(1)	170.7(3)
		N(3)–Ru–Cl(1)	89.7(2)
		N(2)–Ru–Cl(1)	88.2(2)
		N(4)–Ru–Cl(1)	93.3(3)

The cationic molecules are packed in a zigzag manner with anions (ClO_4^-) in between the zip when viewed down the *a*-axis (Fig. 3). Both the hydrogens of the pendant amine group are involved in hydrogen bonding. Hydrogen H(6A) forms hydrogen bonds with the chlorine atom Cl(1) $[-x+3/2, y-1/2, -z+1/2]$ of Ru–Cl, N(6)–H(6A)···Cl(1) = 2.543 Å while H(6B) forms hydrogen bonds with the oxygen atom O(2) of

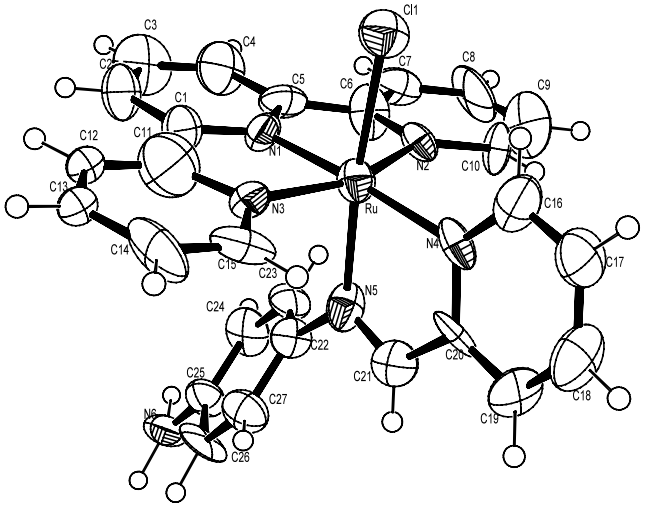

Fig. 2. An ORTEP diagram for $[Ru^{II}(trpy)(L')Cl]ClO_4$ (**1a**). Atoms are drawn at 50% probability.

the translated perchlorate anion moiety, N(6)–H(6B)···O(2) = 2.123 Å (Table 3). The Cl(2)–O(2) distance of 1.372 Å is longer compared to the other Cl–O distances in the ClO_4^- anion which may be due to its involvement in the hydrogen bonding.

3.3. Spectral properties

The ν(C=N) stretching frequency of the coordinated L′ has been observed near 1600 cm^{-1}. The bands due to ionic perchlorate and ν(Ru–Cl) have appeared near 1100/630 and 300 cm^{-1}, respectively.

The ^1H NMR spectra of the free ligands (L) in $CDCl_3$ (Fig. 4(a)) exhibit the signals corresponding to half of the molecule as expected due to the internal symmetry. The complexes (**1a** and **1b**) in DMSO-d^6 solvent display the expected 22 and 26 signals, respectively (Fig. 4(b and c)). The signals due to the NH_2 group [which is absent in the free ligands (Fig. 4(a))], the pendant phenyl ring(s) and the azomethine (–CH=N–) function of L′ appear in isolated regions and are therefore assigned. On the other hand the signals due to the terpyridine ligand and the pyridine fragment of L′ are found to overlap severely which essentially restricts the identification of the individual protons. However, the direct comparison of the intensity of these proton signals with that of the clearly observable NH_2 protons or –CH=N– proton reveals the presence of the calculated number of protons in both the complexes.

Electronic spectral data of the isolated complexes **1a**, **1b**, **2a** and **2b** are listed in Table 4. The complexes display moderately strong MLCT transitions in the visible region ($\lambda_{max} > 500$ nm for **1** and approximately 470 nm for **2**) and strong intra ligand transitions in the UV region (Fig. 5) [34,35]. The observed order of MLCT band energy, **1**(Cl^-) < **2**(H_2O) (Table 4, Fig. 5) is due to relative stabilization of the dπ(Ru) state while moving from $Cl^- \rightarrow H_2O$.

The replacement of one strong π-acidic tridentate trpy ligand from the $[Ru(trpy)_2]^{2+}$core by L′ and Cl^- decreases the MLCT transition energy reasonably {the MLCT transition of $[Ru(trpy)_2]^{2+}$ appears at 478 nm [36]}, however the MLCT transition energy remains almost unaltered when the combination of L′/H_2O is used to replace one trpy group from the $[Ru(trpy)_2]^{2+}$core.

The MLCT transition energy of the aqua derivative, **2a** varies reasonably depending on the nature of the coordinating solvents [37], however little variation has been observed in case of **2b** (Table 4).

The other known ruthenium terpyridine aqua complexes $[Ru(trpy)(L'')(H_2O)]^{2+}$ incorporating analogous

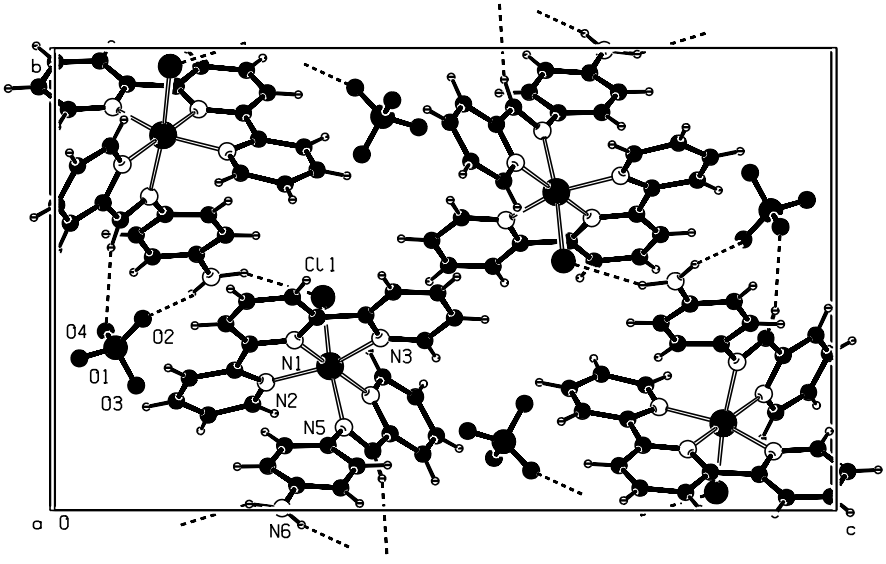

Fig. 3. Packing diagram of the molecule $[Ru^{II}(trpy)(L')Cl]ClO_4$ (**1a**) viewed down the *a*-axis.

Table 3
Hydrogen bonds for **1a** [Å and (°)]

D–H	d(D–H)	d(H···A)	<DHA	d(D···A)	A
N(6)–H(6A)	0.998	2.543	150.65	3.448	Cl(1) [$-x+3/2,\ y-1/2,\ -z+1/2$]
N(6)–H(6B)	0.987	2.123	166.24	3.090	O(2) [$-x+2,\ -y+1,\ -z+1$]

ancillary moieties, L″ = bipyridine [21], bipyrazine [18], azopyridine [15] and 3,6-di(pyrid-2-yl)pyridazine [19] exhibit MLCT transitions at 477, 494, 487–490 and 480–491nm, respectively.

The complexes (**1**) exhibit moderately strong emissions near 590 nm in MeOH–EtOH (1:4 v/v) glass at 77 K from the lowest energy MLCT transitions ($\lambda_{excitation}$: **1a**, 517 nm; **1b**, 520 nm; $\lambda_{emission}$: **1a**, 590 nm; **1b**, 592

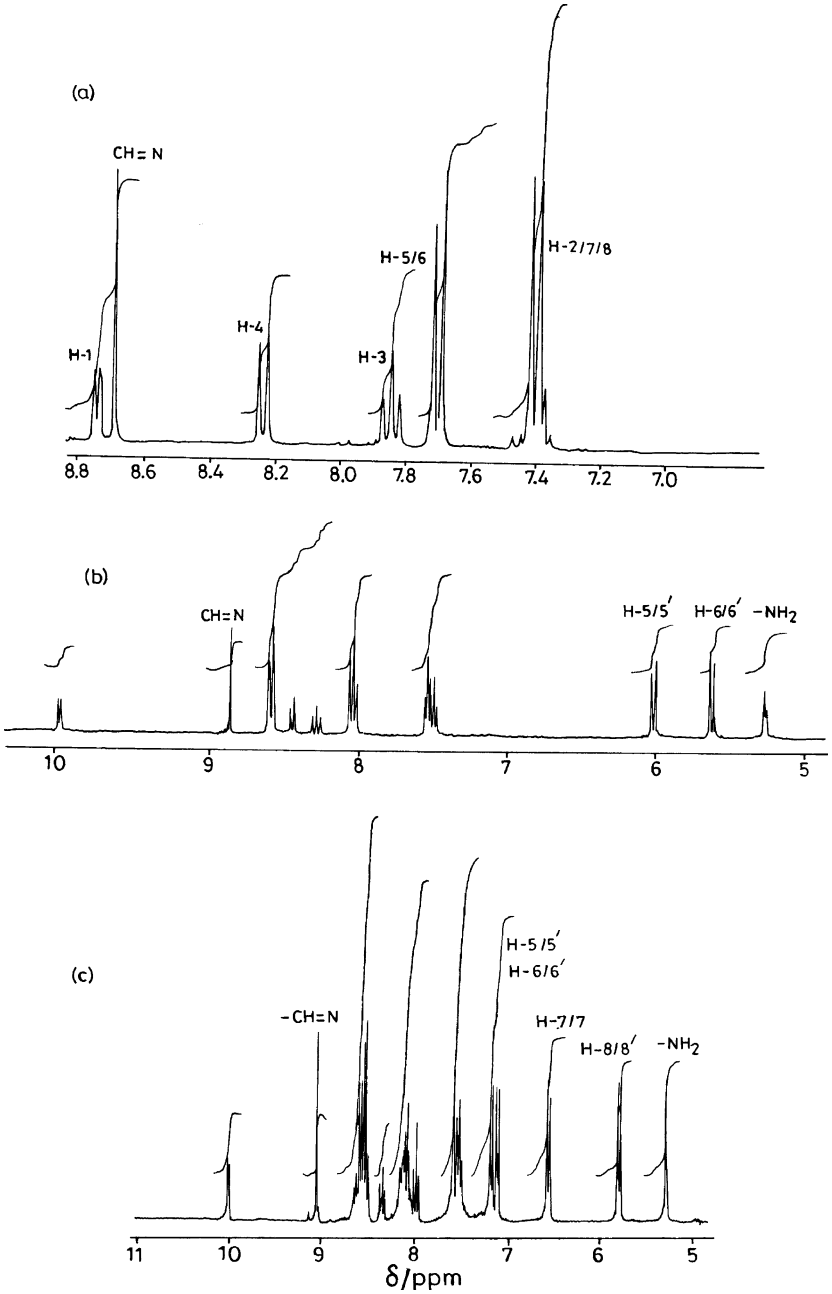

Fig. 4. ^{1}H NMR spectra of: (a) $NC_5H_4CH{=}N{-}C_6H_4{-}C_6H_4{-}N{=}CHC_5H_4N$, L^2 in $CDCl_3$; (b) $[Ru^{II}(trpy)(L')Cl]ClO_4\cdot 2H_2O$ (**1a**); and (c) $[Ru^{II}(trpy)(L')Cl]ClO_4\cdot 2H_2O$ (**1b**) in DMSO-d^6.

Table 4
Electronic spectral data

Complex	UV–Vis λ (nm) (ε, M^{-1} cm^{-1})			
	CH_3CN	CH_3OH	H_2O	DMF
1a	521 (8540) 313 (33 480) 275 (34 090) 234 (35 260) 214 (42 510)			
1b	503 (5890) 314 (41 230) 278 (37 380) 232 (39 970) 213 (47 220)			
2a	471 (6370) 446 (6140) 302 (33 080) 274 (26 310)	475 (6780) 312 (32 000) 274 (25 740)	474 (5590) 310 (26 890) 273 (21 800)	480 (6900) 315 (33 530) 277 (27 510)
2b	473 (7860) 304 (48 870) 280 (32 370)	472 (8430) 304 (50 500) 280 (35 820)	473 (6820) 304 (34 480) 278 (31 800)	474 (9450) 315 (48 870) 285 (36 640)

nm; quantum yield (Φ_{em}): **1a**, 0.03; **1b**, 0.015, Fig. 5, (inset). The observed emissions are believed to have originated from the ^{3}MLCT excited states [38]. The quantum yields (Φ_{em}) of the emission processes were measured in the MeOH–EtOH (1:4 v/v) glass at 77 K relative to $[Ru(bpy)_3]^{2+}$ for which $\Phi_{em} = 0.35$ [39].

3.4. Electron-transfer properties

Redox properties of the complexes **1** and **2** have been studied in acetonitrile and water, respectively using a platinum working electrode at 298 K. Representative voltammograms are shown in Fig. 6. The chloro complexes **1a** and **1b** display reversible ruthenium(III)–ruthenium(II) couples, E°_{298}, V (ΔE_p, mV) at 0.80 (90) and 0.85 (90) versus SCE, respectively. Thus the ruthenium(III)–ruthenium(II) potential increases with the increase in number of phenyl rings in the ligand framework (L′). Although the complexes (**1**) can be coulometrically oxidized to the corresponding ruthenium(III) congeners ($\mathbf{1}^+$), the oxidized species are found to be unstable at room temperature. The observed ruthenium(III)–ruthenium(II) potential of **1** is comparable to that of $[Ru(trpy)(bipyridine)Cl]^+$ (0.81 V) [18] but less anodic compared to those of analogous complexes incorporating other types of *N*,*N*-donors based ancillary functions such as, $[Ru(trpy)\{3,6\text{-di(pyrid-2-yl)pyridazine}\}Cl]^+$ (0.89–1.04 V) [19]; $[Ru(trpy)(azopyridine)Cl]^+$ (1.10–1.24 V) [15] and [Ru(trpy)(2,2′-bipyrazine)Cl] (1.07 V) [18]. Thus the π-acceptor strength of L′ in **1** can be considered to be appreciably closer to that of the bipyridine ligand.

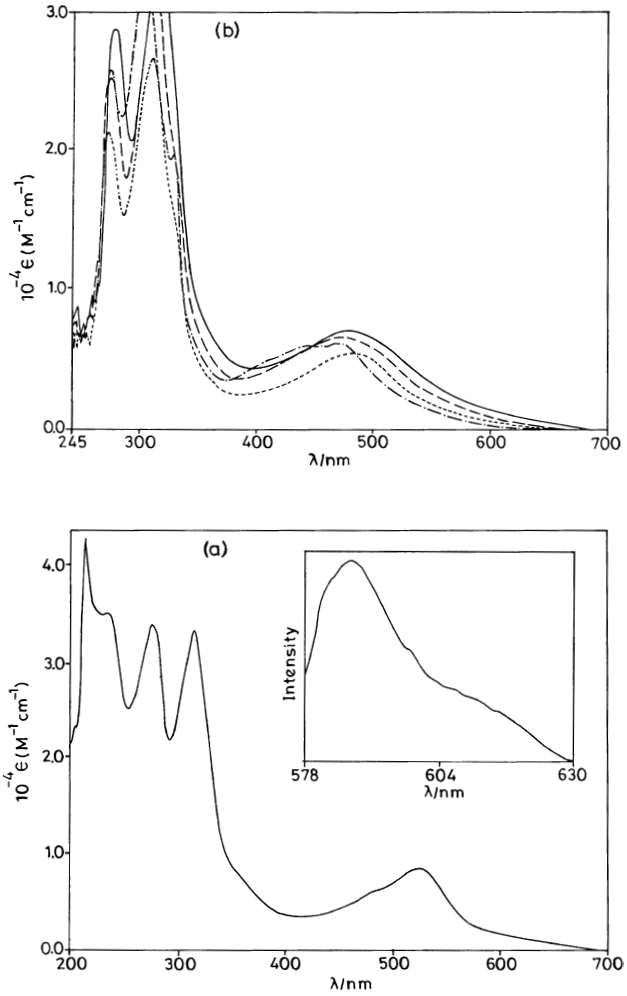

Fig. 5. Electronic spectra of: (a) $[Ru^{II}(trpy)(L')Cl]ClO_4\cdot 2H_2O$ (**1a**) in acetonitrile. Inset shows emission spectrum of $[Ru^{II}(trpy)(L')Cl]ClO_4\cdot 2H_2O$ (**1a**) in EtOH–MeOH 4:1 (v/v) at 77 K; (b) $[Ru^{II}(trpy)(L')(H_2O)](ClO_4)_2\cdot 2H_2O$ (**2a**) in DMF (—), MeOH (----), H_2O (------), CH_3CN (-·-·-).

The complex, **1a** exhibits one irreversible reduction, E_{pc} at −1.09 V and **1b** displays one quasi-reversible reduction, E°_{298}, V (ΔE_p, mV), at −0.96 (190). These are believed to be terpyridine based reductions [40].

Cyclic voltammograms of the aqua species (**2a** and **2b**) have been recorded in aqueous medium in the pH range 1–12. The complexes exhibit one quasi-reversible oxidative response each at the positive side of SCE (Fig. 6(b)). The potentials of the responses are observed to decrease linearly with the increase in pH (Fig. 6(c)). The electron–proton content of the redox processes over the pH range 1–12 have been estimated from the slopes of the experimentally derived potential–pH plots (Fig. 6(c)) [21]. In the pH ranges 1–9 and >9.0, the potentials change at the rate of approximately 60 and 30 mV, respectively per unit change in pH. Therefore, the redox processes in the pH range 1–9 and >9 are associated with $2e^-/2H^+$ and $2e^-/H^+$ oxidation processes, respectively (Eqs. (1) and (2)) [19–21]. The pK_a

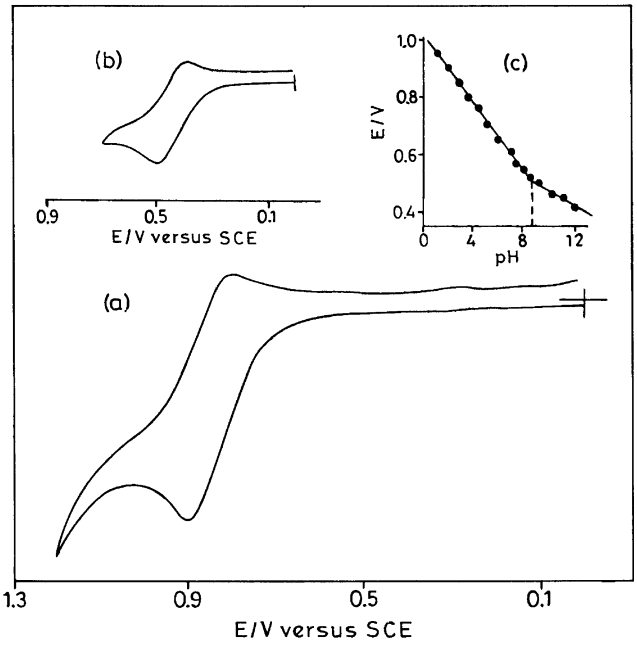

Fig. 6. Cyclic voltammograms of: (a) $[Ru^{II}(trpy)(L')Cl]ClO_4 \cdot 2H_2O$ (**1b**) in acetonitrile; (b) $[Ru^{II}(trpy)(L')(H_2O)](ClO_4)_2 \cdot 2H_2O$ (**2b**) in water at pH 9.5; and (c) variation of Ru^{IV}/Ru^{II} couple with pH in water for **2b**.

values of the complexes **2a** and **2b**, calculated from the intersection point of the two curves in E versus pH graphs (Fig. 6(c)), are 9.0 and 8.7, respectively. The values are in good agreement with the pK_a data (9.1 for **2a** and 9.0 for **2b**) determined separately by

$$[Ru^{II}(trpy)(L')(H_2O)]^{2+} \rightarrow [Ru^{IV}(trpy)(L')(O)]^{2+} + 2e^- + 2H^+ \quad (1)$$

$$[Ru^{II}(trpy)(L')(OH)]^{+} \rightarrow [Ru^{IV}(trpy)(L')(O)]^{2+} + 2e^- + H^+ \quad (2)$$

spectrophotometric titrations using sodium hydroxide. The pK_a values of the similar monoterpyridine aqua complexes $[Ru(trpy)(L'')(H_2O)]^{2+}$, L″ = 2,2′-bipyridine, 1,10-phenanthroline, 2,2′-bipyrazine, 3,6-di(pyrid-2-yl)pyridazine, tetramethylene diamine, and azopyridine are 9.7, 9.6, 8.8, 10.3, 10.2 and 7.9–8.5, respectively [15,18–20]. Thus, as far as the acidity of the coordinated aqua molecule is concerned, the present set of complexes (**2a** and **2b**) are closest to the bipyrazine derivative.

Similar proton coupled electron-transfer processes have been observed in case of bipyrazine [18] and 3,6-di(pyrid-2-yl)pyridazine [20] complexes. However, the bipyridine analogue shows two step processes in the acidic region, $[Ru^{II}(trpy)(bpy)(H_2O)]^{2+} \rightarrow [Ru^{III}(trpy)(bpy)(OH)]^{2+} + e^- + H^+$ and $[Ru^{III}(trpy)(bpy)(OH)]^{2+} \rightarrow [Ru^{IV}(trpy)(bpy)(O)]^{2+} + e^- + H^+$ [21]. On the other hand the azopyridine analogue exhibits $2e^-/2H^+$-transfer process specifically in the highly acidic region [15]. Therefore, electron-transfer behavior of the ruthenium terpyridine aqua species is primarily controlled by the acidity of the coordinated H_2O molecule or in other words the electronic aspect of the ancillary functions.

3.5. *Chemical oxidation of $[Ru^{II}(trpy)(L')(H_2O)]^{2+}$ (**2**) → $[Ru^{IV}(trpy)(L')(O)]^{2+}$ (**3**): role of **3** in catalyzing the water oxidation process*

Chemical oxidation of the aqua complex (**2**) by excess aqueous ceric solution in 1 (N) H_2SO_4 leads to the spontaneous formation of a yellow colored species. The intensity of the MLCT band of $[Ru(trpy)(L)(H_2O)]^{2+}$ near 470 nm is found to decrease systematically on progressive addition of Ce^{IV} solution with the concomitant development of a new band near 320 nm (Fig. 7). The plots of absorbance versus $[Ce^{IV}]/[\mathbf{2}]$ show that approximately 4.0 mole ratio of Ce^{IV}: **2** is needed for the complete oxidation of the aqua species.

Considering the observed electrochemical concerted $2e^-/2H^+$ oxidation process of the aqua complexes in acidic solution (Eqs. (1) and (2)) it can be assumed that the chemical oxidation of **2** also leads to the formation of the same oxo-species, Eq. (3).

$$[Ru^{II}(trpy)(L')(H_2O)]^{2+} + 2Ce^{4+} \rightarrow [Ru^{IV}(trpy)(L')(O)]^{2+} + 2e^- + 2H^+ + 2Ce^{3+} \quad (3)$$

The oxo-complexes (**3**) thus formed are found to reduce back partially to the parent aqua derivatives (**2**). The MLCT band at 474 nm, characteristic of the aqua species, develops slowly with time but levels off before attaining the calculated intensity of the standard aqua species (Fig. 7, inset). The percent conversion of the oxo (**3**) to aqua (**2**) for **3a** and **3b** are calculated to be 63 and 69%, respectively. The further addition of acidic Ce^{+4} solution into the mixture of **2** and **3** oxidizes the solution completely to the oxo-state and the cycle follows. Therefore, the oxo-species is stable only in presence of excess oxidant. The observed partial conversion of oxo to aqua species possibly can account for the need of excess ceric rather than the 1:2 mole ratio of **2**–Ce^{IV} as expected from the stoichiometric oxidation reaction (Eq. (3)). The partial conversion of oxo to aqua species has essentially precluded the isolation of the oxo-complexes in the pure solid state. The observed conversion of the oxo to aqua species and the subsequent reverse reaction, aqua to oxo on further addition of Ce^{4+} can be best explained on the basis of earlier observations [15,17,41] i.e. the involvement of the chemically generated oxo-species in the catalytic water splitting reaction (Scheme 2). It may be noted that in the case of the azopyridine analogue, the oxo complex was found to transform quantitatively to the aqua species and the backward process, aqua to oxo was observed on further addition of Ce^{4+}. Therefore, as far as water splitting is concerned the present oxo-species (Scheme 2) is much less efficient as compared to the corresponding azopyridine deriva-

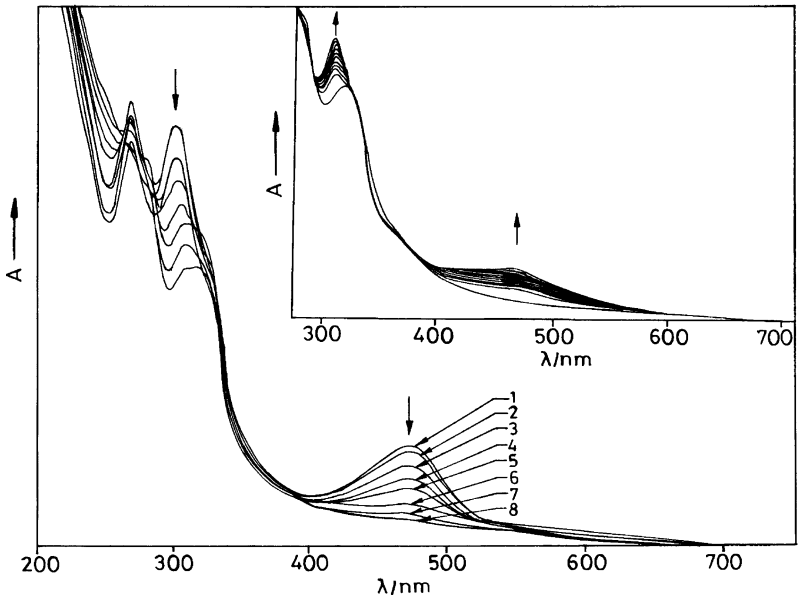

Fig. 7. Change in absorbance of $[Ru^{II}(trpy)(L')(H_2O)](ClO_4)_2\cdot 2H_2O$ (**2a**) as a function of $[Ce^{IV}]$. Ratio of $[Ce^{IV}]$–**2a** = (1) 0:1, (2) 0.5:1, (3) 1:1, (4) 1.5:1, (5) 2:1, (6) 2.5:1, (7) 3:1, (8) 3.5:1. Inset shows time evolution of the electronic spectra of a changing solution of $[Ru^{IV}(trpy)(L')(O)]^{2+}$ (**3a**) → $[Ru^{II}(trpy)(L')(H_2O)]^{2+}$ (**2a**) in water [1 (N) H_2SO_4] at 298 K. The arrows indicate increase or decrease in band intensities as the reaction proceeds.

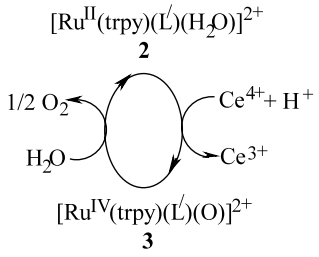

Scheme 2.

tive, which is certainly due to the greater π-acceptor character of the azopyridine function.

3.6. Electrocatalytic oxidation of benzyl alcohol

The cyclic voltammetric experiments of the aqua species $[Ru(trpy)(L')(H_2O)]^{2+}$ (**2**) in the presence of benzyl alcohol have been studied in order to examine the role of the electrogenerated $[Ru(trpy)(L')(O)]^{2+}$ (**3**) towards the oxidaton of benzyl alcohol [18–20,42–44]. The cyclic voltammogram of **2b** at pH 9.58 is shown in Fig. 8. Under identical experimental conditions the voltammogram of benzyl alcohol does not show any appreciable current (Fig. 8). However, the voltammogram of **2** in the presence of benzyl alcohol displays substantially excess anodic current as compared to that of the standard **2** (Fig. 8). Thus the oxidation of **2** to **3** is followed rapidly by the reaction (Scheme 3) and the regenerated **2** is reoxidized before it can diffuse away from the electrode surface.

Therefore, the electrogenerated **3** is involved in catalyzing the benzyl alcohol oxidation process. A similar electrocatalytic behavior has been reported in case of the corresponding bipyrazine and 3,6-di(4-methylpyrid-2-yl)pyridazine complexes [18–20]. Here catalytic current increases with the increase in ratio of [benzyl alcohol]/[**2**] as expected and maximum catalytic current is observed in case of 25:1 ratio of [benzyl alcohol]/[**2**]. The catalytic effect has been quantifiedly based on the experimentally observed excess current (i_{ex}) with respect to the current only due to the catalyst (i_{ct}) (same catalyst concentration has been used for both the standard and the mixture containing the substrate) at a particular potential (Eq. (4)) (Fig. 8) [45]. Here i_o is the observed current for

$$i_{ex} = i_o + i_d - i_{ct} \quad (4)$$

the mixture and i_d is the difference in current between the catalyst and the catalyst + substrate at the concerned base line potential. The turnover numbers (t) of the processes

$$t = i_{ex}/i_{ct} \quad (5)$$

(Scheme 3; Fig. 8) calculated by using Eq. (5) are found to be 2.7 and 2.3 for **3a** and **3b**, respectively. Further studies on the catalytic aspect of **3** are in progress.

4. Conclusion

The role of α,α′-diimine based ancillary (L′) functions in the ruthenium monoterpyridine [Ru-trpy] core (**1**–**3**) have been scrutinized with special reference to the chemical and electrochemical behaviors of the oxo species $[Ru(trpy)(L')(O)]^{2+}$ (**3**). The ruthenium(III)–

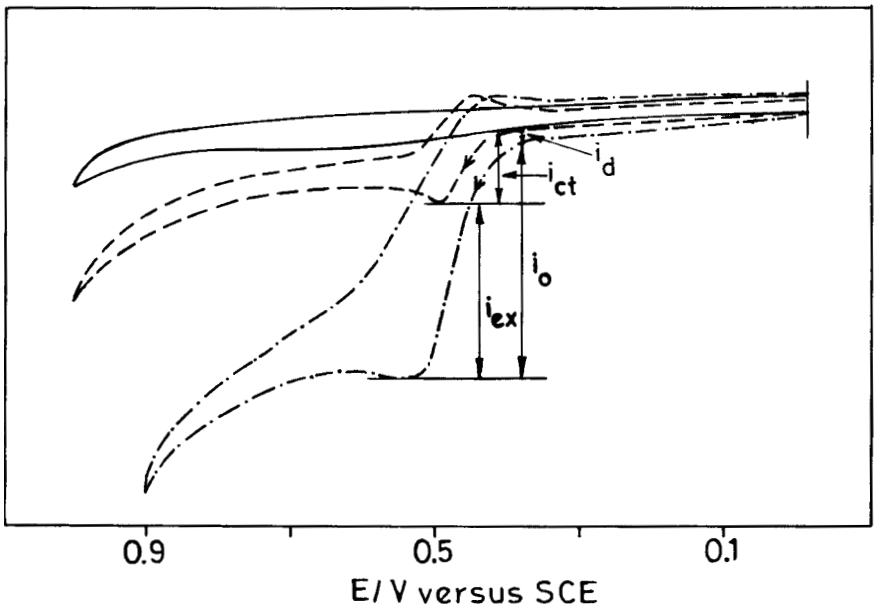

Fig. 8. Cyclic voltammograms of benzyl alcohol in water (20.32×10^{-3} M) (—); $[Ru^{II}(trpy)(L')(H_2O)](ClO_4)_2 \cdot 2H_2O$ (**2b**) in water at pH 9.58 (0.96×10^{-3} M) (----) and the mixture of the two taken at the same concentrations (-·-·-).

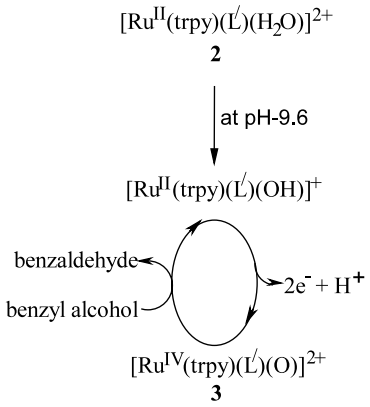

Scheme 3.

ruthenium(II) potential of the chloro species $[Ru(trpy)(L')(Cl)]^+$ (**1**) is comparable to that of the corresponding bipyridine complex but less anodic compared to the analogous complexes incorporating 3,6-di(pyrid-2-yl)pyridazine, bipyrazine and azopyridine ancillary functions. The aqua complex $[Ru(trpy)(L')(H_2O)]^{2+}$ (**2**) undergoes one-step-$2e^-/2H^+$ and $2e^-/H^+$ transformations in the acidic and basic regions, respectively to the corresponding oxo-species $[Ru(trpy)(L')(O)]^{2+}$ (**3**) like the bipyrazine and 3,6-di(pyrid-2-yl)pyridazine derivatives. The chemically generated oxo-species (**3**) catalyzes the water oxidation process like the azopyridine derivative but much less efficiently. The electrochemically generated oxo-species (**3**) is found to be effective in catalyzing the oxidation of benzyl alcohol like the bipyrazine and 3,6-di(pyrid-2-yl)pyridazine derivatives. The present study therefore emphasizes the serious impact of the electronic aspect of the ancillary functions in directing the reactivity pattern of the ruthenium monoterpyridine aqua species.

5. Supplementary material

Crystallographic data for the structural analysis have been deposited with the Cambridge Crystallographic Data Center, CCDC Nos. 170396–170397 for compounds **1a** and L^1. Copies of this information may be obtained free of charge from The Director, CCDC, 12 Union Road, Cambridge, CB2 1EZ, UK

Acknowledgements

Financial support received from the Council of Scientific and Industrial Research, New Delhi, India, is gratefully acknowledged. The X-ray structural studies were carried out at the National Single Crystal Diffractometer Facility, Indian Institute of Technology, Bombay. Special acknowledgement is made to the Regional Sophisticated Instrumental Center, RSIC, Indian Institute of Technology, Bombay, for providing NMR facility.

References

[1] F. Scandola, C.A. Bignozzi, M.T. Indelli, in: K. Kalyanasundaram, M. Gratzel (Eds.), Photosensitization and Photocatalysis

Using Inorganic and Organometallic Compounds, Kluwer, Dordrecht, 1993, p. 161.
[2] K. Kalyanasundaram, Coord. Chem. Rev. 28 (1989) 2920.
[3] J.P. Sauvage, J.P. Collin, J.C. Chambron, S. Guillerez, C. Coudret, V. Balzani, F. Barigelletti, L. De Cola, L. Flamigni, Chem. Rev. 94 (1994) 993.
[4] C.M. Hartshorn, K.A. Maxwell, P.S. White, J.M. DeSimon, T.J. Meyer, Inorg. Chem. 40 (2001) 601.
[5] B. Gholamkhass, K. Koike, N. Negishi, H. Hori, K. Takeuchi, Inorg. Chem. 40 (2001) 756.
[6] I.V. Yang, H.H. Thorp, Inorg. Chem. 40 (2001) 1690.
[7] V.M. Hultgren, A.M. Bond, A.G. Wedd, J. Chem. Soc., Dalton Trans. (2001) 1076.
[8] H. Sugimoto, K. Tsuge, K. Tanaka, J. Chem. Soc., Dalton Trans. (2001) 57.
[9] B.K. Santra, M. Menon, C.K. Pal, G.K. Lahiri, J. Chem. Soc., Dalton Trans. (1997) 1387.
[10] J. Zadykowicz, P.G. Potvin, Inorg. Chem. 38 (1999) 2434.
[11] M. Kurihara, S. Daniele, K. Tasuge, M. Sugimoto, K. Tanaka, Bull. Chem. Soc. Jpn. 71 (1998) 867.
[12] A. Doveletoglou, S.A. Adeyemi, T.J. Meyer, Inorg. Chem. 35 (1996) 4127.
[13] M. Ebadi, A.B.P. Lever, Inorg. Chem. 38 (1999) 467.
[14] B. Mondal, S. Chakraborty, P. Munshi, M.G. Walawalkar, G.K. Lahiri, J. Chem. Soc., Dalton Trans. (2000) 2327.
[15] B. Mondal, M.G. Walawalkar, G.K. Lahiri, J. Chem. Soc., Dalton Trans. (2000) 4209.
[16] B. Mondal, H. Paul, V.G. Puranik, G.K. Lahiri, J. Chem. Soc., Dalton Trans. (2001) 481.
[17] N.C. Pramanik, K. Pramanik, P. Ghosh, S. Bhattacharya, Polyhedron 17 (1998) 1525.
[18] A. Gerli, J. Reedijk, M.T. Lakin, A.L. Spek, Inorg. Chem. 34 (1995) 1836.
[19] V.J. Catalano, R.A. Heck, C.E. Immoos, A. Ohman, M.G. Hill, Inorg. Chem. 37 (1998) 2150.
[20] V.J. Catalano, R.A. Heck, A. Ohman, M.G. Hill, Polyhedron 19 (2000) 1049.
[21] K.J. Takeuchi, M.S. Thompson, D.W. Pipes, T.J. Meyer, Inorg. Chem. 23 (1984) 1845.
[22] V. Balzani, A. Juris, M. Venturi, S. Campagna, S. Serroni, Chem. Rev. 96 (1996) 759.
[23] M.D. Ward, Chem. Soc. Rev. (1995) 121.
[24] D. Gust, T.A. Moore, L. Moore, Acc. Chem. Res. 115 (1993) 5975.
[25] A.M. Barthram, R.L. Cleary, R. Kowallic, M.D. Ward, Chem. Commun. (1998) 2695.
[26] T. Wada, K. Tsuge, K. Tanaka, Angew. Chem., Int. Ed. Engl. 39 (2000) 1479.
[27] T. Wada, K. Tsuge, K. Tanaka, Inorg. Chem. 40 (2001) 329.
[28] S. Chakraborty, P. Munshi, G.K. Lahiri, Polyhedron 18 (1999) 1437.
[29] W.J. Stratton, D.H. Busch, J. Am. Chem. Soc. 80 (1958) 1286.
[30] B.P. Sullivan, J.M. Calvert, T.J. Meyer, Inorg. Chem. 19 (1980) 1404.
[31] G.M. Sheldrick, SHELXS-97, Program for Crystal Structure Solution and Refinement, University of Göttingen, 1997.
[32] S. Chakraborty, M.G. Walawalkar, G.K. Lahiri, J. Chem. Soc., Dalton Trans. (2000) 2875.
[33] A.E.M. Boelrijk, J. Reedijk, J. Mol. Catal. 89 (1994) 63.
[34] D.A. Bardwell, A.M.W. Cargill Thompson, J.C. Jeffery, J.A. McCleverty, M.D. Ward, J. Chem. Soc., Dalton Trans. (1996) 873.
[35] R.R. Ruminsky, S. Underwood, K. Vallely, S.J. Smith, Inorg. Chem. 37 (1998) 6528.
[36] C.R. Hecker, A.K.I. Gushurst, R.D. McMillin, Inorg. Chem. 30 (1991) 538.
[37] M.D. Ward, Inorg. Chem. 35 (1996) 1712.
[38] L.M. Vogler, K.J. Brewer, Inorg. Chem. 35 (1996) 818.
[39] R. Alsfasser, R.V. Eldik, Inorg. Chem. 35 (1996) 628.
[40] G.B. Deacon, J.M. Patrick, B.W. Skelton, N.C. Thomas, A.H. White, Aust. J. Chem. 37 (1984) 929.
[41] S. Goswami, A.R. Chakravarty, A. Chakravorty, J. Chem. Soc., Chem. Commun. (1982) 1288.
[42] E.L. Lebeau, T.J. Meyer, Inorg. Chem. 38 (1999) 2174.
[43] W. Kutner, T.J. Meyer, R.W. Murray, J. Electroanal. Chem. 195 (1985) 375.
[44] L. Roecker, T.J. Meyer, J. Am. Chem. Soc. 109 (1987) 746.
[45] G.K. Lahiri, S. Bhattacharya, S. Goswami, A. Chakravorty, J. Chem. Soc., Dalton Trans. (1990) 561.